2014 IEEE/RSJ International Conference on
Intelligent Robots and Systems (IROS 2014)
September 14-18, 2014, Chicago, IL, USA

Advances in Fibrillar On-Off Polymer Adhesive: Sensing and Engagement Speed *

Nicholas Wettels, *Member, IEEE* and Aaron Parness, *Member, IEEE*

Abstract— **ON-OFF adhesives can benefit manufacturing and space applications by providing the capability to selectively anchor two surfaces together repeatedly and releasably without significant preload. Two key areas of concern are speed of engagement and sensing the quality of that engagement. Here we describe a dual-purpose proximity and tactile sensor for the contact surfaces of robotic systems. Using infrared emitters and combinations of wide and narrow angle detectors, this device combines proximity and force sensing to seamlessly transition from a pre-contact to contact state. As an inherently low-power device, it is amenable to mobile robotic applications. We also present results showing this engagement can occur very rapidly, making it useful in high-throughput manufacturing and dexterous manipulation tasks.**

I. Introduction

When conducting a gripping/grappling operation, there is a chain of useful points to consider: 1) the proximity of the gripper to the object to manage when adhesive engagement should occur, 2) rapid engagement of the adhesive to facilitate grip at the moment of contact, and 3) assessment of the quality of the grip. Addressing these points, there is utility in combining a range and force sensor in a common package for real time operation; these combined data are generally useful for algorithms that fuse visual and tactile information to resolve object proximity and contact forces.

The contribution of this paper is to show demonstration of rapid attachment and engagements sensing that have not been previously covered and are of value to all classes of adhesive-based grippers. Results from the adhesive sensor, algorithms, and the gripping mechanism will be presented.

II. Background

For grappling objects in orbit, traditional kinematic grasp theory implies the need to achieve a force-closure grasp based on multiple friction forces [1]. For example, a two-jaw gripper can only grip a pipe if each jaw reaches sufficiently around the pipe to react the forces of the opposite jaw. This enables objects that are difficult or impossible to manipulate with conventional grippers (i.e. solar panels, fuel tanks, etc.) to be handled effectively. Using an ON-OFF adhesive gripper (ON-OFF and gecko-adhesive terms are used interchangeably here) allows large surfaces on a target to serve as potential grapple points. The space-compatible adhesive structure can be turned on or off by applying a slight shear force relative to the plane of attachment. This adhesive mimics the geometry and performance characteristics of the adhesive structures found on the feet of gecko lizards. Adhesive levels range from near zero on rough surfaces to more than 25 kPa of normal adhesion and 75 kPa of shear adhesion on smooth surfaces like glass.

The gecko-adhesive based grippers have specific application areas in manufacturing, for instance Glass panel handling: The ON-OFF adhesive can engage in 1 – 10 msec versus 100 – 1,000 msec (based on authors' experience and discussions with industry) for typical suction cup grippers, resulting in an increase in throughput.

Several space-based applications are also of interest including: orbital debris mitigation, satellite servicing, spacecraft inspection, and rendezvous and docking systems [2].

A. Gecko-Like Adhesives

The toes of a gecko have microscopic and nano-scopic hairs that adhere to smooth surfaces by way of van der Waals forces [3]. Synthetic microstructures that replicate this phenomenon have been produced by several laboratories, each with their own recipe, properties, and trade-offs [4-6], none of which yet equal the performance of the biological example. The structure used in this work is shown in Figure 1 and is comprised of wedge-shaped microscopic stalks that protrude perpendicularly from the surface. NASA-JPL's adhesive can be turned ON-OFF using a slight sliding motion (see Fig. 1). Directional, gecko-inspired adhesives are suitable for such applications because they require little energy for attachment and detachment, work on many surfaces, and can undergo many attach/release cycles. Because the adhesives rely predominantly on van der Waals forces to stick, they are compatible across a wide range of environments, including extreme temperatures and in vacuum.

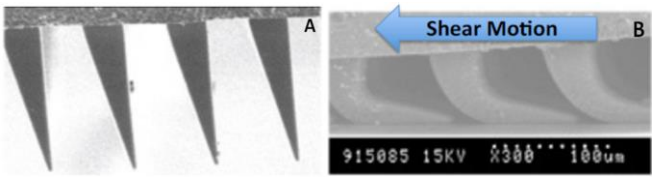

Figure 1: Scanning electron microscope images of the adhesive in the OFF and ON states. A) The adhesive in the OFF state. Only the tips of the triangular structure make contact with the surface resulting in a low real area of contact relative to the apparent area of contact. B) With a slight shear motion, the adhesive is turned to the ON state. The flexible wedges bend over creating a high real area of contact, significant van der Waals forces, and thus high levels of adhesion.

*Research was carried out at the Jet Propulsion Lab, California Institute of Technology, under contract with the National Aeronautics and Space Administration. Government Sponsorship Acknowledged.

N. Wettels and A. Parness are with the NASA Jet Propulsion Laboratory, Pasadena, CA 91109 USA (phone: +1-213-477-0710, email: wettels@jpl.nasa.gov or nick.wettels@gmail.com, email: aaron.parness@jpl.nasa.gov)

We have constructed and tested a variety of gripping systems using the ON-OFF adhesive. Common features of these systems include:

- Ability to affix to a wide variety of industrial surfaces including glass, metals, composites, and painted surfaces; anything from a very smooth to matte finish
- Extreme reusability (>30,000 ON-OFF cycles); can remain ON or OFF for > 1year
- High force capability >10 kPa of adhesion on most surfaces; typical normal (adhesion) to shear force ratio is 1:3 [2]
- Adhesive effect is temperature, radiation and vacuum invariant; dirt resistant [7, 8]

B. Previous Work in Proximity and Contact Sensing

Typical sensory systems for range/ proximity and contact or force involved a laser or LED-phototransistor system coupled with limit-switches, force sensitive resistors and/or a load cell beneath the sensing surface. Here we roll all of these sensing capabilities into a single device.

The proximity detection method is similar to those used by commercial IR-based sensors [9]; a phototransistor receives an IR signal reflected off an object from a transmitting, co-located LED/ laser diode. The system then uses triangulation between the sensor and emitter to determine object distance within a specified range. Here, instead of triangulation, we take advantage of the large amount of available real estate under the gecko-adhesive pad by implanting multiple phototransistors and LEDs (geometry and calculations described later in Methods). This configuration also surmounts the "dead-zone" problem triangulation-based sensors face when objects are close.

In the realm of force sensing, a wide variety of transduction mechanisms including optics, capacitance, piezoresistance, ultrasound, and conductive polymers have all yielded viable solutions, but often only for limited environments or applications. For example, most MEMS sensors provide good resolution and sensitivity, but lack the robustness for many applications outside the laboratory; reviews of tactile sensing can be found in [10-12]. The elastomeric optical tactile sensor presented in this paper achieves robustness by avoiding the placement of delicate sensors or electrical connections in harm's way.

The use of optics in tactile sensor is not new; several attempts have been made to use either camera based or electro-optic modalities in tactile sensing. The camera-based approaches generally involve tracking patterns or the position of landmarks on the inner surface of an elastomer [13, 14]. Other approaches involve modulating the signal between a light emitting element and a light sensor [15, 16] or coupling optical waveguides [17]. The approach presented in this work is closest to [16] and [17] where modulation of the mean free path of photons to a receiver modulates the beam.

III. Methods

A. Rapid Engagement

As discussed, one of the key features of an adhesive-based grippers for manufacturing and orbital applications is rapid attachment. In a manufacturing environment, suction-based grippers can require up to 1,000 msec of 'engagement' time during which the gripper is stationary. A two-pad rapid engagement gripper was built to observe and demonstrate the engagement speed of gecko adhesive grippers.

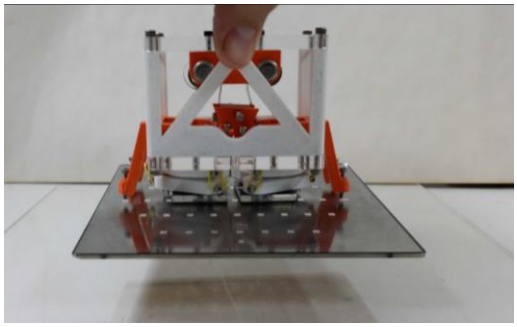

Figure 2: The rapid engagement gripper lifting a glass plate. The outer portion of the trigger mechanism (orange) lifts off the surface on contact with the surface, freeing the springs to retract and engage the gecko adhesive pads.

Our gripper (Figure 2) uses two adhesive pads with the preferred loading direction facing inwards. A cable links the pair, connecting to each pad in its center to prevent the application of moments to the adhesive. This cable is connected through a swivel to a set of constant force coil springs that are extended and held in place by a trigger mechanism in the OFF state. The trigger mechanism is activated when both sides of a scissor linkage make contact with a surface, freeing the pin that is holding the constant force springs extended. As the springs retract, they apply load to the cable that connects the gecko adhesive pads and turns the gripper ON, as shown in Figure 1 and in the supplemental video attachment.

B. Sensing

B.1 .Construction

The device consists of a set of distributed infrared (IR) phototransistors and light emitting diodes (LEDs) atop a printed circuit board (PCB).

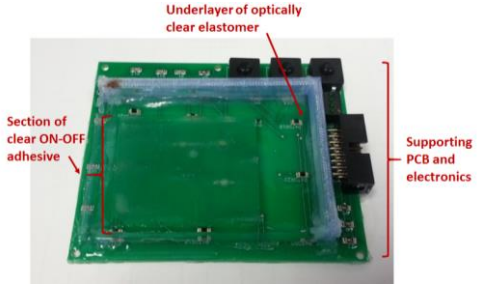

Figure 3: PCB with phototransistors and LEDs overmolded with Solaris and EPM-2421 gecko-adhesive layers.

Two LEDs (940 nm, 40 mW/sr output, 24 degree viewing angle) provide illumination for 6 narrow angle phototransistors (Pxtor) (770 – 1090nm sensitivity, 870 nm peak, 26 degree viewing angle) and 6 wide angle phototransistors (720 – 1200 nm sensitivity, 940 nm peak). A 4 mm thick layer of optically clear Solaris silicone

elastomer (shore A 15, Smooth-On.) is molded over the top of the device with a 1 mm thick, 3x4 cm clear strip of gecko-adhesive (EPM-2421 silicone, NuSil Technologies) bonded atop the Solaris layer (see Fig. 3).

The phototransisors are arranged in series with load resistors and voltage output is routed to a shielded cable and connected to a data acquisition enviroment using a National Instruments NI-USB 6218 and Matlab Data Acquisition Toolbox custom program, sampling data at 120 Hz with an 8-point moving average filter.

B.2. Measurement Principle

When the light is emitted from the LED (in 24-degree cone), it will undergo diffuse reflection off the surface of object above the device (see Fig. 4). This results in omni-directional reflection angles due to surface irregularities.

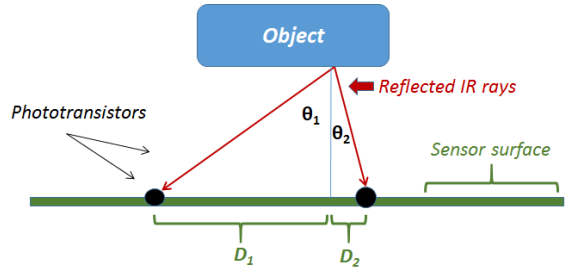

Figure 4: Light cast from the IR LEDs (not shown) from the PCB will be received at multiple angles from by multiple phototransitors (2 shown here). Based on knowledge of receipt angles and locations of sensors relative to one another inferrences about object distance can be made.

The light will also undergo intensity loss due to absorption and scattering as it transmits through the various lengths of materials (elastomer and air):

$$I = I_0 e^{-ax} \quad (1)$$

where Io = the intensity of the light passing through a medium; a = the absorption coefficient of the material (wave length dependent) and x = the distance the light must travel through a given material. Because we have chosen clear materials, these effects are minor in comparison to the dominant reflective response of the device. As an object approaches the sensor system, the "field-of-view" of the object will increase, causing the amount of reflected IR light from that object to increase. The narrow angle set of phototransistor's output will change depending upon which angle or range of angles IR light is received (Fig. 5). When an object of a given size is far away, the reflected light will have a narrow (small) angle of return. As the object approaches, more light is collected from a wider spread of angles, causing the photo-current of the Pxtors to increase. Eventually the object will contact the surface of the device; normal forces will compress the soft underlayer of elastomer, causing photo-current to increase further, albeit not as dramatically. To further sense this effect, we also examine the response of wide-angle phototransistors. These Pxtors do not have the angular discriminability that the narrow angle Pxtors do, but capture reflected light from a wider field-of-view. As objects are contacted, the path of light from the LED to the phototransistors is deformed, changing its intensity.

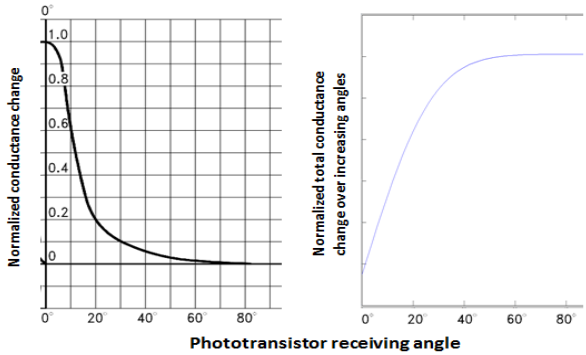

Figure 5: The narrow-angle phototransistors relate voltage data a manufacturer-defined curve, to convert these voltages into angles that are useful for force and distance calculation.

These changes in intensity will contain information about the contacted object such as its center of pressure and force.

In summary:

- Narrow-angle Pxtors → Range calculation
- Wide-angle Pxtors → Augment force calculation

While the device is not designed to sense shear forces explicitly per se (it is not clear how shear loading effects would be captured by this planar device), it can sense "engagement" of the gecko-adhesive. When shear force is applied to the adhesive after a relatively small normal pre-loading force, the hairs of the gecko-adhesive bend over, causes a dramatic optical change in the material. In the instance of a clear adhesive, the material becomes white-translucent and reflects and scatters more light generated by the IR LEDs.

Several assumptions are made about the sensor-object interaction: 1) The IR LEDs produce significantly more radiation than ambient, 2) objects in question have an appreciable IR reflectivity, 3) objects are relatively flat (do not have large features that protrude towards the sensor), 4) object area is not significantly smaller than the area of the sensor board and 5) the contact environment is sterile (e.g. space) – gecko-adhesives do not function well in dusty environments and non-uniform fouling of the surface would impact measurements.

Our goals are to build and test a prototype that can discriminate through various ranges of proximity of space-grade materials and contact conditions: 1) 40 cm from a surface to 2) contacting the surface, 3) up to the exertion of +100N of force on the unit and 4) shear force engagement detectability. This proximity range was chosen because it is roughly an order of magnitude larger than the sensor surface dimensions and force range was chosen because this represents more than sufficient pre-load the device would need for shear force engagement.

B.3. Proximity Sensing

The advantage of our algorithm is that it uses comparison of relative intensities of the received light to judge distance. This makes the algorithm invariant to ambient conditions

and lateral object dimensions (provided the object is large enough to be "seen") and surface types (e.g. reflective vs. non-reflective), are within the previously discussed constraints.

Proximity of an incoming object is determined by translating the amount of photo-current produced from each phototransistor to a span of angles from reflected IR rays based on object field-of-view. This is translated into object distance using trigonometry and known distances of the sensors between one another. Photo-current is determined from the voltage divider arrangement of the Pxtors and scaled from 0 to 1 based on the dark (ambient) current and maximum possible photo-current:

$$I_p = \frac{V_{out}(V_{cc}-1)}{R_{Load}} \quad (2)$$

$$I_{pScale} = \frac{i_p - i_{pZero}}{i_{pMax} - i_{pZero}} \quad (3)$$

The maximum angle of incipient IR light is determined by integrating the Gaussian function (Fig. 5 – from manufacturer data sheet) of phototransistor angle versus scaled photo-current input; the inverse is taken using Matlab's spline function to ultimately relate photo-current to angles:

$$Y = 1.011\ \mathrm{erf}\left(\frac{\theta - 0.6294}{14.7}\right) \quad (4)$$

$$\theta = Y^{-1} \quad (5)$$

Where *erf* is the error function. The algorithm then checks if the calculated angle is outside the bounds of 2 to 30 degrees. If it is, this phototransistor is not used in subsequent calculations because angular resolution outside these bounds is poor. The least-squares fit of an object's range (R) is calculated from multiple (*i,j)* phototransistor pair angles (Fig. 5) using the Moore-Penrose pseudo-inverse and the distance (D) between them by:

$$R(\theta) = \begin{bmatrix} D_{12} \\ \vdots \\ D_{ij} \end{bmatrix} \begin{bmatrix} \tan\theta_1 & + & \tan\theta_2 \\ \vdots & & \vdots \\ \tan\theta_i & + & \tan\theta_j \end{bmatrix}^{-1} \quad (6)$$

Range determination was evaluated at 40.6, 20.3, 10.2, 3.8 and 0 cm (contact), repeated 3 times each, and 50 data points collected at each location using four typical space-grade objects/ materials of varying size: 1) woven astro-quartz (25 x 28 cm), 2) Space Shuttle thermal tile (18 x 28 cm), 3) carbon fiber panel (16.5 x 10 cm), 4) solar panel (30.5 x 90.5 cm); (sensor board is 7.5 x 6 cm). Range data were processed via linear calibration as well as a neural network calibration (artificial neural network (ANN) described below).

B.4. Force and Engagement Sensing

To relate phototransistor output to normal force, the relative intensities of the wide-angle (and narrow-angle) are processed by an artificial neural network. ANNs are able to cope with the non-linear response of the sensor due to rubber deformation from the object. We anticipate faithful representation of normal forces because the elastomer will deform like a spring in the normal direction. To determine if cross axis sensitivity from shear forces would be a confounding problem, each material was pressed in the sensor board (0 – 175N) and a variety of shear forces (+/- 20N, x and y directions) were applied as well. In a further attempt to confuse the machine learning algorithm, data from the range sensitivity trials were included as well. Forces were recorded with the previously mentioned data acquisition system and an ATI Omega-85, 6-DOF load cell.

The ANN used here is a three-layer back-propagation perceptron [18] using Matlab's Neural Network Toolbox. First we construct a linear combination of N input variables (Eqn. 7):

$$A_j = \sum_{i=1}^{N} W_{ji}\, X_i + W_{j0} \quad (7)$$

where parameters Wji refer to the weights and Wj0 refers to the biases of the activation function Aj. These M basis function outputs are linearly combined to form the K outputs for which the system was trained:

$$A_k = \sum_{j=1}^{M} W_{kj}\, Z_j + W_{k0} \quad (8)$$

The toolbox employed the Levenberg-Marquardt back-propagation algorithm to tune the weights and biases of the ANN. Prior to training, the primary data sets were divided into three sets: 1) a working set (70%), 2) a validation set consisting of 15% of randomly chosen data to prevent over-fitting; and 3) a test set of 15% randomly chosen data used to measure the ANN's ability to generalize after training.

A neural network classifier was also used to examine if the system could discriminate between three states of shear force induced gecko-adhesive engagement: 1) No engagement, 2) Intermediate engagement and 3) Full engagement. Such states are shown below in Fig. 6. In an effort to confuse the training algorithm, shear engagement was performed amidst a variety of normal forces (75N +/- 75N). A confusion matrix was produced to show false positive and false negative misclassifications of the test set to evaluate network performance.

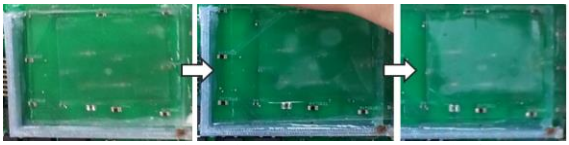

Figure 6: Top) Regular photo showing No Engagement (Left), Intermediate Engagement (Middle) and Full Engagement (Right)

IV. RESULTS

A. Rapid Engagement

With a total of 5 cm^2 of gecko adhesive, the gripper was able to lift and manipulate 1 kg glass plates to any orientation. The two-pad rapid engagement mechanism was able to grip in 16 msec as observed through high-speed video. Using larger gecko adhesive pads or tiling multiple pairs together allows larger loads to be handled. Engagement speed is determined by how quickly load can be transferred from the constant force springs to the adhesive pads.

B. Sensing

B.1. Proximity Sensing

Figure 7 shows results from a typical trial of thermal tiling: raw sensor output and uncalibrated algorithm output are shown. The algorithm error is largely dominated by a static off-set. Linearly calibrated results showed an appreciable amount of variation between object classes (R^2 = 0.701; RMSE = 8.39 cm):

$$R_{cal} = 0.9638\,R - 14.09 \quad (9)$$

Figure 8 shows neural network calibrated data and much improved results (R^2 = 1.00; RMSE < 1e-3 cm); though the drawback of using ANNs to calibrate data is they then become highly dependent on the strength of the parent training set and may not generalize well when encountering new object sets.

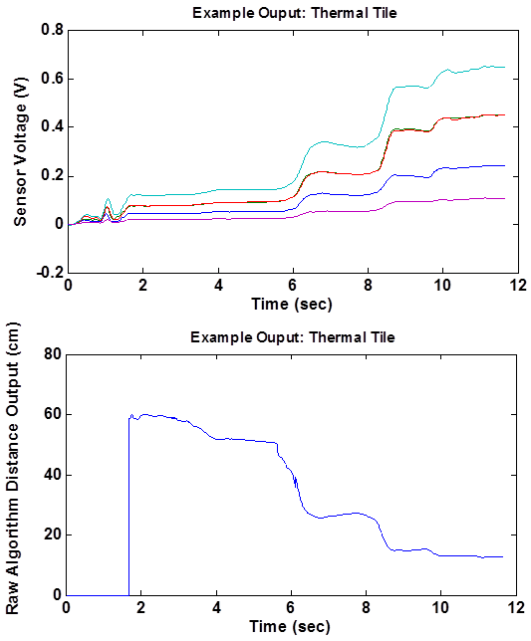

Figure 7: Top) Sample "zeroed" sensor output during trial using the Thermal Tile; output varies as some sensors are located beneath the adhesive strip and some are not. Bottom) Algorithm output for same data; large offset is clear and data above 60 cm are forces to zero due to insufficient change in received angle

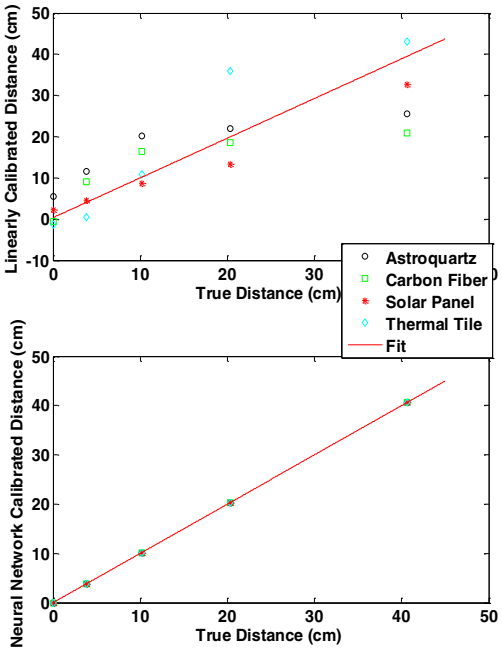

Figure 8: Top) Linearly calibrated data output (all sets). Bottom) ANN calibrated data (all sets)

B.2. Force and Engagement Sensing

Fig. 9 shows sample data from one of the normal force sensing validation sets (carbon fiber panel featured here.

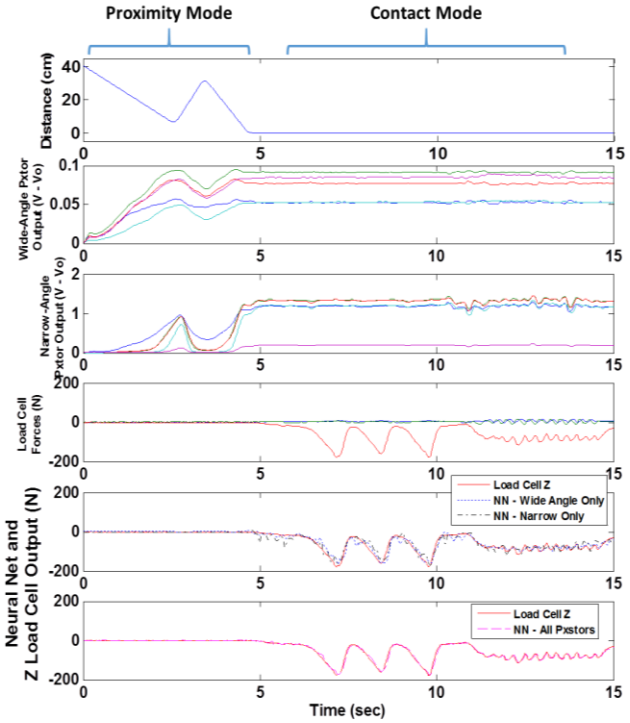

Figure 9: First (from Top)) Distance plot showing regions of contact and non-contact; Second) Wide-angle phototransistor output; Third) Narrow-angle phototransistor output; Fourth) Load cell output up to 200N axial compressive force with variations at 80 +/- 20N axially and 0 +/- 20N shear (both directions); Fifth) Individual narrow and wide-angle ANN output overlaid on normal force; Sixth (Bottom)) All phototransistor set ANN overlaid on normal force.

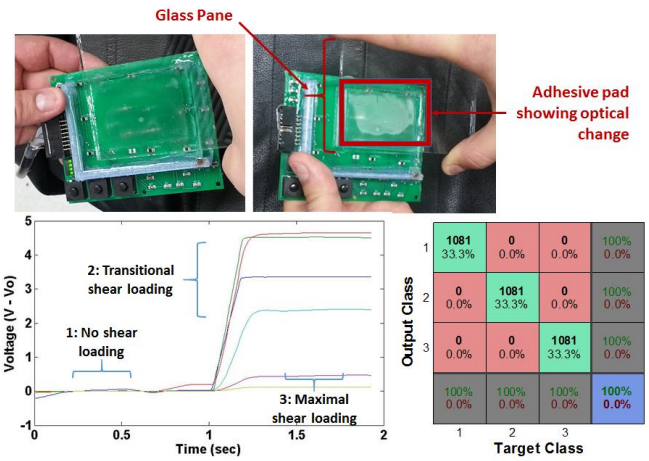

Figure 10: Top Left) Device with no gecko-adhesive engagement; Top Right) Full adhesive engagement showing optical change; Bottom Left) Transition of narrow-angle sensor response between two states. Bottom Right) ANN classifier confusion matrix: Target classes represent different states; green blocks show number and percent correct classification, red blocks show misclassifications (false positives upper right, false negatives lower left; grey blocks represent totals; blue block is average classification; per block # instances are on top, % below.

The ANN using all phototransistors was best able to discriminate contact as well as normal forces near 200N (R^2 = 0.985; 7.99 % error over full-scale range) as opposed to individual phototransistor sets (wide-angle only: R^2 = 0.940; 18.8 % error; narrow-angle only: R^2 = 0.906; 20.4 % error). Figure 10 demonstrates discriminability and the drastic change in sensor output due to the engagement effect.

V. Discussion

We have successfully shown proof-of-concept for rapid attachment and sensing mechanisms for a gecko-inspired adhesive. Regarding rapid pad engagement, the pads only need to move approximately 30 μm to engage [4] resulting in a fast-actuating system: 16 msec in this study as verified by high-speed camera. Using a fast robotic arm instead of a human arm, it is estimated that the gripper can engage in less than 10 msec.

The sensing modality was able to demonstrate changes in sensor performance relative to proximity, normal forces and shear force-based engagement of the device. Training algorithms also showed robustness to shear forces during normal force discrimination and normal forces during engagement discrimination. There was a large overestimation offset error in the raw proximity calculation. This was likely due to the low number of narrow-angle sensors, which were also not optimized for placement and measurement errors in the manual distance data collection.

The good performance of the force an engagement sensing can be attributed to the clear separation of domains of data with regard to proximity (lower ~0 to 20% of sensor output change), normal force (~20 to 25% output) and engagement (upper 75% of output). During adhesive engagement, the folding over of the fibrillar stalks produced a frustrating path for the IR light, causing much of it to scatter back to the phototransistor; the obvious optical effect we see. The engagement classifier also only had 3 states to discriminate from as well and as Fig. 10 shows, these data are clearly separated. It is not likely much more granularity would be needed in a usable device, but it if were, more error would be present.

Next steps for this project include fabricating a beta version that integrates the quick-actuating gripper and sensing mechanism, sensor optimization, and replacing the discrete wide-angle sensors with high-density charge-coupled device arrays as well as more rigorous testing and characterization of the device (e.g. continuous distance measurement, normal force hysteresis testing); these challenges do not seem prohibitive given the design and availability of materials for the device.

References

[1] Shimoga K. B., "Robot grasp synthesis algorithms: a survey," *Intl. J. of Robotics Research,* vol. 15, pp. 230–266, 1996.

[2] Parness A., Heverly M., Hilgemann E., Wettels N., Hilgendorf T., White V., Kennedy B., "ON-OFF Adhesive Grippers for Earth-Orbit," *in Proc. of American Institute of Aeronautics and Astronautics Conference*, San Diego, CA USA, 2013

[3] H. Hamaker, "The london-van der waals attraction between spherical particles," Physical, 1937.

[4] K. Autumn, A. Dittmore, D. Santos, M. Spenko, and M. Cutkosky, "Frictional adhesion: a new angle on gecko attachment," Journal of Experimental Biology, vol. 209, no. 18, pp. 3569–3579, 2006.

[5] A. Asbeck, S. Dastoor, A. Parness, L. Fullerton, N. Esparza, D. Soto, B. Heyneman, and M. Cutkosky, "Climbing rough vertical surfaces with hierarchical directional adhesion," IEEE ICRA, pp. 1–6, 2009.

[6] A. Parness, "Microstructured adhesives for climbing applications," Stanford University Thesis, 2010.

[7] P. Day, M. Cutkosky, R. Greco, and A. McLaughlin, "Effects of He++ ion irradiation on adhesion of polymer microstructure based dry adhesives," Nuclear Science and Engineering, vol. 167, no. 3, 2011.

[8] http://www.nusil.com/products/engineering/aerospace /ultra low outgassing TM/potting and encapsulating .aspx.

[9] http://www.sharpsma.com/webfm_send/1208

[10] Dahiya R., Metta G., Valle M., Sandini G., "Tactile Sensing – From Humans to Humanoids," IEEE Transactions on Robotics, Vol. 26(1), pp 1-20, 2010.

[11] Lee M. H. and Nicholls H. R., "Tactile sensing for mechatronics-A state of the art survey," Mechatronics, vol. 9, pp. 1-31, 1999.

[12] Melchiorri C., "Tactile Sensing for Robotic Manipulation," Ramsete: Lecture Notes in Control and Information Sciences, vol. 270, Springer, Berlin, 2001.

[13] Hristu D., Ferrier N., and Brockett R.W., "The performance of a deformable-membrane tactile sensor: basic results on geometrically-defined tasks," IEEE Internation Conference on Robotics and Automation, San Francisco, vol. 1, pp. 508-513, 2000.

[14] Ohka M., "Optical three-axis tactile sensor", Mobile Robots: Towards New Applications, ARS Journal and Springer, ch. 6, 2007.

[15] Crosnier, J. "Grasping systems with tactile sense using optical fibres," Robot Sensors, vol. 2: Tactile and Non-Vision. IFS Publications/ Springer-Veriag, New York, pp 209-217, 1986.

[16] Persichetti A., Vecchi F., and Carrozza M.C., "Optoelectronic-based flexible contact sensor for prosthetic hand application," IEEE Conference on Rehabilitation Robotics, Netherlands, pp. 415-420, 2007

[17] Ferraris E., Van Gijseghem T., Yan C., Van Hoe B., Van Steenberge G, Van Daele P., Dubruel P., Reynaerts D., Embedding of fibre optic sensors within flexible host, *Proc. Int'l Conf. Multi-Mater. Micro Manufact. (4M)/Int'l Conf. Micro Manufact. (ICOMM)*, pp. 351-354, 2009

[18] Bishop C.M. Neural Networks for Pattern Recognition, Oxford: University Press, 1995